

Infrared Study of the Pressure-Induced Isostructural Metallic Transition in $\text{Mo}_{0.5}\text{W}_{0.5}\text{S}_2$

Published as part of The Journal of Physical Chemistry virtual special issue "D. D. Sarma Festschrift".

Elena Stellino, Francesca Ripanti,* Giacomo Nisini, Francesco Capitani, Caterina Petrillo, and Paolo Postorino*

Cite This: *J. Phys. Chem. C* 2021, 125, 15503–15509

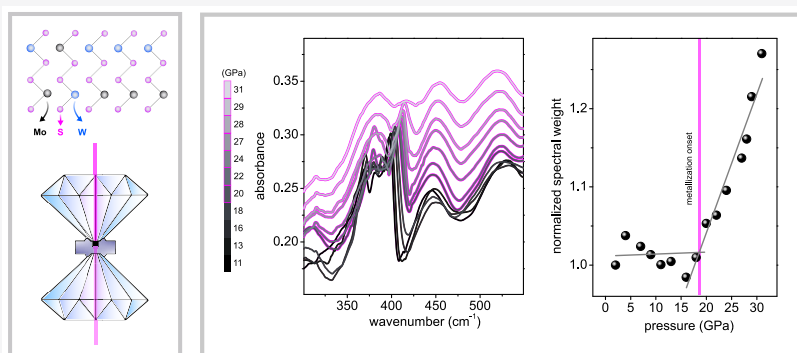
Read Online

ACCESS |

Metrics & More

Article Recommendations

Supporting Information



ABSTRACT: Ternary compounds of transition metal dichalcogenides are emerging as an interesting class of crystals with tunable electronic properties, which make them attractive for nanoelectronic and optoelectronic applications. Among them, $\text{Mo}_x\text{W}_{1-x}\text{S}_2$ is one of the most studied alloys due to the well-known and remarkable features of its binary constituents, MoS_2 and WS_2 . The band gap of this compound can be modeled varying Mo and W percentages in the sample, and its vibrational modes result from a combination of MoS_2 and WS_2 phonons. In this work, we report transmission measurements on a $\text{Mo}_{0.5}\text{W}_{0.5}\text{S}_2$ single crystal in the far-infrared range. Absorbance spectra collected at ambient conditions enabled for the first time a classification of the infrared-active phonons, complementary to Raman studies. High-pressure measurements allowed the study of the evolution of both the lattice dynamics and the free carrier density up to 31 GPa, suggesting the occurrence of an isostructural semiconductor-to-metal transition above 18 GPa, in very good agreement with the theoretical calculation reported in the literature.

INTRODUCTION

Among two-dimensional (2D) materials, in the last few years transition metal dichalcogenides (TMDs) have proven to be one of the most promising classes of crystals in terms of both applications and fundamental studies. Semiconducting TMDs are characterized by a graphene-like layered lattice, easily exfoliable down to atomic-thick crystals^{1–3} but, at variance with graphene, their band structure exhibits finite band gaps in the eV scale, which are attractive for electronic devices.^{4–6} One of the most remarkable features of TMDs, as well as many others 2D materials, is the key role of the interlayer interaction in determining the sample properties,^{7–9} such as the strong relationship between the electronic structure and the number of layers. Indeed, in most semiconductors, a progressive increase of the band gap is observed as the number of layers reduces, and an indirect-to-direct band gap crossover arises when bilayer samples are scaled down to monolayers.^{10–12}

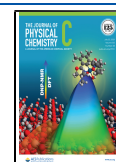
Because of the high heterogeneity and the outstanding structural and electronic properties of isomorphic semi-

conducting TMDs, the possibility to design and produce heterostructures (formed by stacking together monolayers of different crystals) and alloys (synthesized by directly mixing two different TMDs) with different band gaps has emerged as an appealing strategy to tune and tailor the band structure of these materials for nanoelectronic and optoelectronic applications. In this framework, ternary compounds have been synthesized in which the metal or the chalcogen contributions are adjusted with different atoms from the same element group.^{13,14}

Received: March 17, 2021

Revised: June 21, 2021

Published: July 9, 2021



$\text{Mo}_x\text{W}_{1-x}\text{S}_2$ is one of the most investigated TMD alloys due to the vast amount of studies on its binary constituents MoS_2 and WS_2 .^{15–20} The bulk crystal shows a 2H phase and is formed by stacking together monolayer alloys via van der Waals interactions. The monolayer alloy contains one MoW plane sandwiched by two S planes, represented as S-Mo/W-S. Recent work on $\text{Mo}_x\text{W}_{1-x}\text{S}_2$ has proven that the electronic band gap at ambient conditions can be tuned by modifying the percentage of Mo and W atoms in the lattice.^{21,22} Raman measurements have also been performed, varying the number of layers and the stoichiometric composition, to characterize the vibrational modes of the sample.^{23,24}

The application of pressure is a powerful tool to probe the interlayer interactions in $\text{Mo}_x\text{W}_{1-x}\text{S}_2$ and to explore the tunability of the electronic and structural properties. Indeed, experimental and theoretical reports have already demonstrated that pressure can modulate the band structure of TMDs in general^{25,26} and in particular of MoS_2 and WS_2 .^{27–31} In MoS_2 a metallization has been observed at ~ 19 GPa, accompanied by a structural distortion from 2H_c to 2H_a phase.^{27,32} Similarly, in WS_2 a metallic transition occurs at ~ 22 GPa but, opposite to the previous case, the lattice remains isomorphic.²⁸ High-pressure Raman measurements on $\text{Mo}_{0.5}\text{W}_{0.5}\text{S}_2$ have suggested the absence of structural transitions up to 40 GPa.³³ Regarding the electronic properties, instead, in a recent article by Dong et al.³⁴ a semiconductor-to-metal transition was predicted below 30 GPa for $\text{Mo}_{1-x}\text{W}_x\text{S}_2$ alloys through theoretical calculations. The metallization pressure was found to be dependent on both the number of layers and the Mo/W percentage in the sample. In particular, for bulk $\text{Mo}_{0.5}\text{W}_{0.5}\text{S}_2$ the authors suggested the onset of the transition above 20 GPa.

Here, we report high-pressure transmission measurements on $\text{Mo}_{0.5}\text{W}_{0.5}\text{S}_2$ in the far-infrared (FIR) range, where simultaneous information on the lattice dynamics, complementary to Raman studies, and on the pressure-induced increase of the carrier density is accessible. This work classifies for the first time the infrared-active modes of $\text{Mo}_{0.5}\text{W}_{0.5}\text{S}_2$ at ambient conditions, analyzes their response under pressure, confirming the absence of structural transitions up to 31 GPa, and observes an abrupt increase of the carrier density above 18 GPa, associated with the onset of a semiconductor-to-metal transition.

EXPERIMENTAL SECTION

$\text{Mo}_{0.5}\text{W}_{0.5}\text{S}_2$, MoS_2 , and WS_2 single crystals were provided by HQ-graphene. All measurements were performed on fresh-cut samples, directly cleaved from the macroscopic crystal to obtain flakes a few microns thick with a clean surface. It is worth noticing that, since the typical thickness of single-layer TMDs is ~ 0.7 nm, in the present case we safely work in the bulk limit.

Room-temperature infrared transmission measurements were performed at the beamline SMIS of the SOLEIL synchrotron both at ambient pressure (on all of the samples) and over the 0–30 GPa range (only on $\text{Mo}_{0.5}\text{W}_{0.5}\text{S}_2$).

In the Diamond Anvil Cell (DAC), diamonds with a culet of $250\ \mu\text{m}^2$ were separated by a preindented stainless steel $50\ \mu\text{m}$ thick gasket in which a hole of $125\ \mu\text{m}$ diameter was drilled. The exfoliated sample was positioned in the hole together with CsI as a pressure transmitting medium³⁵ and a ruby chip to measure the pressure through the ruby fluorescence

technique.³⁶ The measured sample was $50\ \mu\text{m}^2$ in area and $2\text{--}3\ \mu\text{m}$ in thickness.

Measurements were performed using a Thermo Fisher iS50 interferometer equipped with a solid-substrate beamsplitter. Synchrotron edge radiation was employed as a light source. Custom-made $15\times$ Cassegrain objectives with a large working distance allowed one to focus and then to collect the transmitted radiation, finally detected by a liquid-helium-cooled bolometer detector.

Raman and photoluminescence measurements at ambient conditions were carried out on $\text{Mo}_{0.5}\text{W}_{0.5}\text{S}_2$, MoS_2 , and WS_2 , using a Horiba LabRAM HR Evolution microspectrometer with a 532 nm laser as a light source. The radiation was focused on a $2\ \mu\text{m}^2$ spot on the sample by a $100\times$ objective and collected by a CCD detector. Further details are provided in ref 37.

RESULTS AND DISCUSSION

Vibrational Modes at Ambient Conditions. Infrared transmission measurements at ambient conditions were performed on $\text{Mo}_{0.5}\text{W}_{0.5}\text{S}_2$, WS_2 , and MoS_2 crystals in the $100\text{--}600\ \text{cm}^{-1}$ range. To reduce the interference effects between the sample surfaces, each crystal was exfoliated on a diamond window, thus minimizing the discontinuity of the refractive index at the substrate interface. Measurements of the background intensity, $I_0(\omega)$, were preliminarily carried out on the bare diamond. The sample transmitted intensity, $I(\omega)$, was then measured once the crystals were positioned on the diamond, allowing the determination of the absorbance spectra $A(\omega) = -\ln[I(\omega)/I_0(\omega)]$. Raman measurements were also collected in the same frequency range as a reference. The comparison between absorbance and Raman spectra of $\text{Mo}_{0.5}\text{W}_{0.5}\text{S}_2$, WS_2 , and MoS_2 is shown in Figure 1.

The absorbance spectrum of $\text{Mo}_{0.5}\text{W}_{0.5}\text{S}_2$ is characterized by the presence of four distinct bands between 300 and $450\ \text{cm}^{-1}$. By comparing it with the $A(\omega)$ spectra of WS_2 and MoS_2 , the peaks at ~ 350 and $\sim 380\ \text{cm}^{-1}$ can be assigned to the E_{1u} - WS_2 -like and the E_{1u} - MoS_2 -like modes, respectively.^{38,39} The larger bandwidth observed for the alloy peaks can be attributed to disorder effects, which are less important in the binary crystals. It is interesting to notice that, although Mo and W atoms are present in the sample with the same percentage, the intensity of E_{1u} - MoS_2 -like is far larger than that of E_{1u} - WS_2 -like. We recall that the infrared phonon intensity is proportional to the square of the first derivative of the dipole moment with respect to the normal mode coordinates. The dipole moment is related to the Born effective charge tensor, i.e., the first derivative of the polarization per unit cell with respect to the atomic displacements. On the basis of the density functional theory calculations reported in the literature,⁴⁰ the Born charges (defined as one-third of the trace of the tensor in Cartesian coordinates) of Mo and W, for in-plane displacements, are in a 2:1 ratio, suggesting a four-times higher intensity of MoS_2 -like mode compared with WS_2 -like one. The less intense peak at $\sim 365\ \text{cm}^{-1}$ between the two E_{1u} phonons may correspond to the disorder-activated longitudinal acoustic (DALA) phonon mode,³³ while the broad band at $\sim 410\ \text{cm}^{-1}$ could be identified with the convoluted A_{1g} modes from MoS_2 and WS_2 .²⁴ Interestingly, both the DALA and the A_{1g} -like modes, whose symmetries are not compatible with the infrared selection rules, do not appear in the binary crystals but can be activated by disorder effects in the ternary compound.

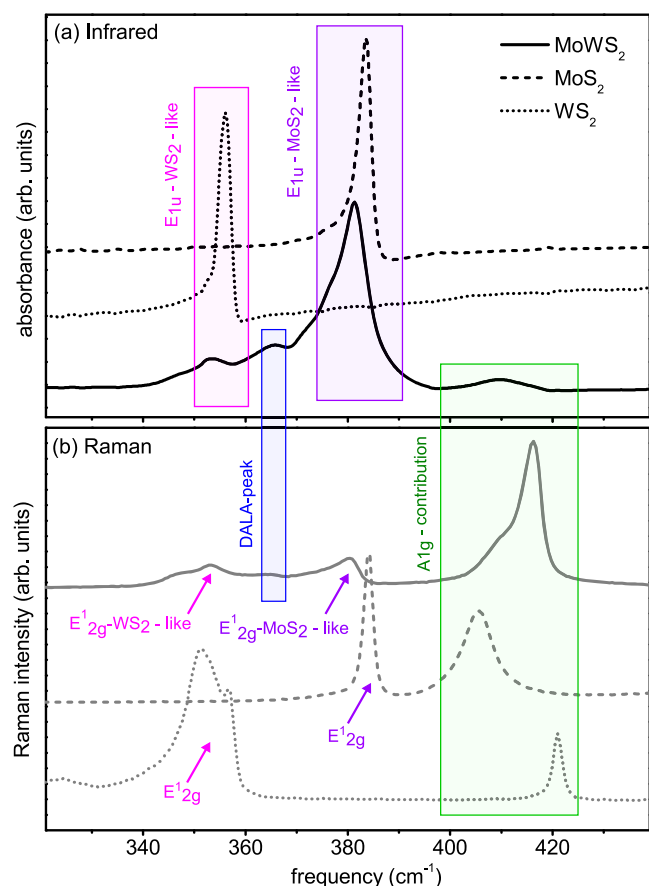


Figure 1. Infrared (a) and Raman (b) spectra of $\text{Mo}_{0.5}\text{W}_{0.5}\text{S}_2$ (continuous lines), MoS_2 (dashed lines), and WS_2 (dotted lines). Magenta and purple areas highlight the contributions of $\text{Mo}_{0.5}\text{W}_{0.5}\text{S}_2$ coming from the IR-active phonons of MoS_2 and WS_2 (E_{1u}). Blue and green areas highlight the contributions of $\text{Mo}_{0.5}\text{W}_{0.5}\text{S}_2$ coming from the IR-inactive, disorder-activated modes of MoS_2 and WS_2 (A_{1g} DALA, see text).

Vibrational Modes under High Pressure. Room-temperature transmission measurements on a $\text{Mo}_{0.5}\text{W}_{0.5}\text{S}_2$ single crystal were performed in the 100–600 cm^{-1} range on increasing pressure from 0 to 31 GPa. The background

intensity, $I_0(\omega)$, was measured with the DAC filled by the hydrostatic medium (CsI) only. The sample transmitted intensity, $I(\omega)$, was then collected once the crystal was loaded into the cell to obtain the absorbance, $A(\omega)$, at each pressure. Interference fringes due to multiple reflections between the diamond surfaces through the hydrostatic medium were observed in $A(\omega)$ spectra. The reduced number of oscillations and the frequency dependence of both the period and the amplitude of the oscillations prevent an effective subtraction in the spectra.

The absorbance spectra on increasing pressure in the 350–430 cm^{-1} range, where the phonon contribution is dominant, are shown in Figure 2. Although the overall intensity of the peaks is reduced with respect to the out-of-cell measurements, a comparison with the spectra reported in Figure 1 allows the identification of the principal bands associated with E_{1u} - WS_2 -like ($\sim 350 \text{ cm}^{-1}$), DALA ($\sim 370 \text{ cm}^{-1}$), and E_{1u} - MoS_2 -like ($\sim 380 \text{ cm}^{-1}$) vibrational modes. In the in-cell measurements, the A_{1g} -like contributions, visible at ambient conditions at $\sim 410 \text{ cm}^{-1}$, are probably hindered by the interference fringes. Notice that, due to the alloyed nature of the compound, the relative intensity of the peaks may slightly vary depending on the measured point of the sample. In particular, disorder activated modes may be favored in regions where the crystal order is reduced. By comparing Figures 1 and 2, the relative intensity of the DALA mode is higher in the first case than in the second one. Since the investigated samples and the regions of the sample surface are different for in-cell- and out-of-cell-measurements, this effect can be ascribed to a different impact of configurational disorder.

As the pressure increases up to 31 GPa, the peak positions regularly shift toward higher frequencies, confirming the absence of structural transitions, as already suggested by Raman measurements.³³ The peak intensities above ~ 20 GPa undergo a progressive lowering until completely vanishing at 31 GPa.

Electronic Properties at Ambient Conditions. Thin $\text{Mo}_{0.5}\text{W}_{0.5}\text{S}_2$ crystals, mechanically exfoliated on a SiO_2 -coated Si substrate, were analyzed through micro-Raman measurements to determine the number of layers (N) of each flake (see Supporting Information, SI). Photoluminescence (PL) measurements at ambient conditions were then performed to

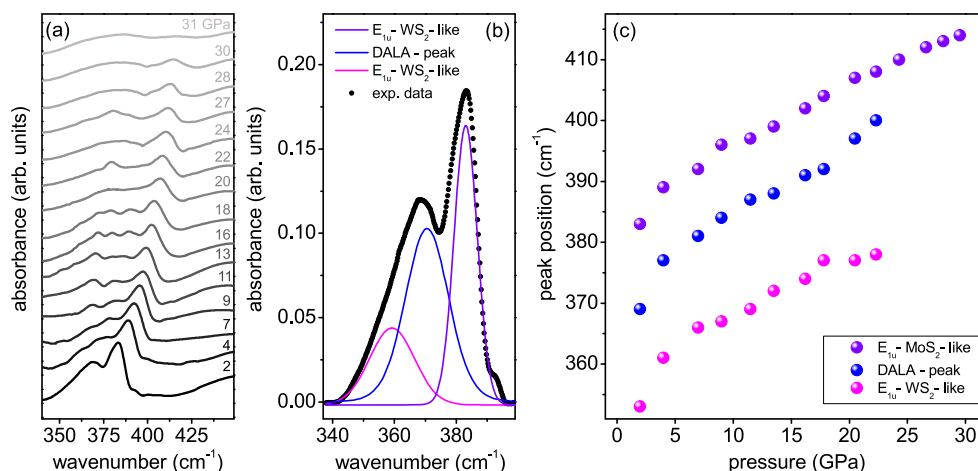


Figure 2. (a) Absorbance spectra of $\text{Mo}_{0.5}\text{W}_{0.5}\text{S}_2$ at increasing pressure from 2 to 31 GPa. Spectra are vertically shifted for sake of clarity. (b) Experimental phonon-peaks at 2 GPa (black dots) fitted with a sum of three Voigt functions. (c) Peak positions as a function of pressure. WS_2 -like- E_{1u} and DALA peaks are no longer distinguishable above 23 GPa.

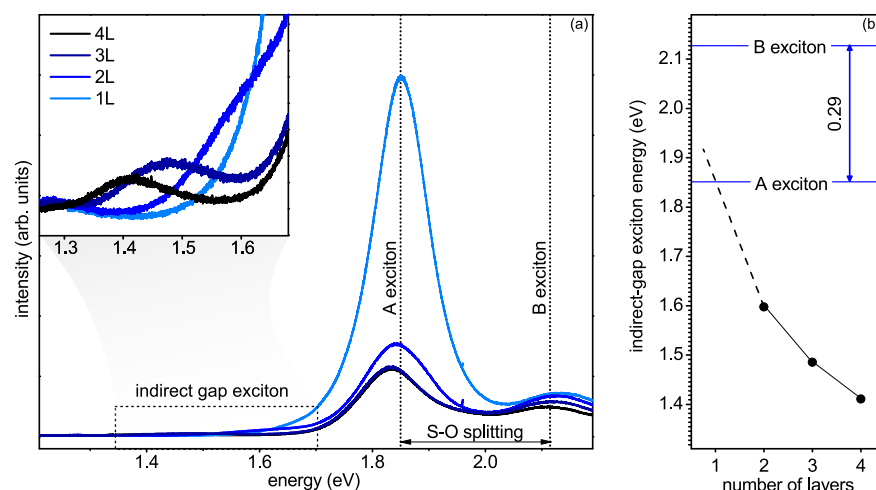


Figure 3. (a) PL spectrum of $\text{Mo}_{0.5}\text{W}_{0.5}\text{S}_2$ samples with a different number of layers. (b) Energy of the exciton associated with the indirect gap as a function of the number of layers.

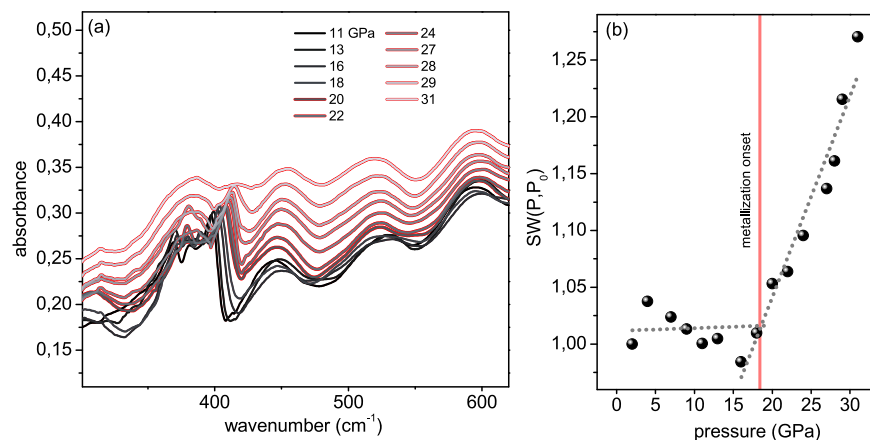


Figure 4. (a) Absorbance spectra of $\text{Mo}_{0.5}\text{W}_{0.5}\text{S}_2$ from 11 to 31 GPa. Above 20 GPa, spectra with a red contour are characterized by increasing spectral weight. (b) Normalized spectral weight ($\text{sw}(P, P_0)$) as a function of pressure. Linear fits in the 2–20 GPa and the 16–31 GPa ranges are reported as dotted lines.

characterize the electronic properties of the sample as a function of N . PL spectra for mono-, bi-, tri- and four-layer samples are reported in Figure 3. The energy of the PL bands in the bulk sample is identical to that of the four-layer sample, although the overall intensity is significantly lower. The spectrum of multilayers samples exhibits three distinct bands: the one at lower energy (~ 1.4 – 1.5 eV) corresponds to the exciton associated with the indirect-gap transition, the most intense one at ~ 1.85 eV is the A exciton, and the one at ~ 2.1 eV is the B exciton with the latter two related to direct transitions.⁴¹ The energy difference between the peaks associated with A and B excitons corresponds to the spin-orbit splitting of the valence band of the crystal. In the monolayer, the well-known transition from indirect to direct gap occurs, and the indirect transition band is no longer visible in the spectrum.

The comparison between the PL spectra of $\text{Mo}_{0.5}\text{W}_{0.5}\text{S}_2$, MoS_2 , and WS_2 (see SI) clearly shows that all the electronic features of the ternary compound lie at halfway between its basic constituents. In particular, in the bulk sample we measured an indirect gap of ~ 1.4 eV, a direct gap of ~ 1.85 eV, and a spin-orbit splitting of ~ 0.29 eV.⁴¹ Indeed, as widely demonstrated in the literature,²¹ the optical band gap of

alloyed crystals strongly depends on the Mo/W ratios and continuously tunable band gap can be achieved by controlling the percentage of transition metal atoms in the sample.

Electronic Properties under High Pressure. To study the evolution of the electronic properties of $\text{Mo}_{0.5}\text{W}_{0.5}\text{S}_2$ as a function of pressure, we analyzed the spectral weight in the far-infrared range at increasing pressure values. This quantity indeed accounts for the low-energy electronic transitions and, thus, allows monitoring a possible insurgence of the metallic regime.

As shown in Figure 4a, the $A(\omega)$ spectra in the FIR region are almost superimposed up to ~ 18 GPa. On further increasing pressure, the overall absorption intensity rises and the phonon peak intensity reduces. The first effect may arise from a rapid increase of the free electron density due to the insurgence of a Drude band at zero frequency. Indeed, as in most semiconducting TMDs, in $\text{Mo}_{0.5}\text{W}_{0.5}\text{S}_2$ the high pressure reasonably drives a progressive reduction of the band gap responsible for the semiconductor-to-metal transition. Correspondingly, the intensity of the vibrational modes decreases since the optical response of the free electrons shields the phonon contribution in the FIR absorption.

To quantitatively characterize the metallization process, we define at each pressure the absorption spectral weight $sw(P) = \int_{\omega_m}^{\omega_M} A(\omega) d\omega$.^{42,43} A simple application of the Drude model proves that in the low-frequency limit, i.e., $\omega/\Gamma \ll 1$ (with $\Gamma = c/\tau$ and τ is the Drude relaxation time), the absorbance is simply proportional to the square root of the DC conductivity σ_0 and ω , $A(\omega) \propto \sqrt{\sigma_0 \omega}$. Since σ_0 is proportional to the carrier density n , the last relation demonstrates that the increase in the FIR absorbance is directly related to the increase of n .^{44,45} Figure 4b reports the values of the normalized spectral weight $sw(P, P_0) = sw(P)/sw(P_0)$ up to 31 GPa, where $P_0 = 2$ GPa and the integration limits are $\omega_m = 200 \text{ cm}^{-1}$ and $\omega_M = 700 \text{ cm}^{-1}$. The integration is not performed over the 350–450 cm^{-1} range where the phonon contribution is predominant. The normalized spectral weight, almost constant at low pressure, undergoes a significant increase around 20 GPa, associated with an increase of the charge carrier density n . To identify the onset of the metallization process, two independent linear fits were performed in the 2–20 and the 16–31 GPa ranges (see Figure 3b): the ordinate of the fitting lines crossing point, $P_M = 18 \pm 1$ GPa, could be assumed as a reference pressure value to describe the beginning of the metallic transition, where actually a strong increase of the spectral weight occurs.⁴⁶ It is worth underlining that P_M reasonably underestimates the effective metallization pressure by a few GPa. Indeed, the increase in the charge carrier density might arise when the band gap is not completely closed but is reduced down to $\sim k_B T$, allowing the electrons in the valence band to be thermally promoted in the conduction band.

The obtained results display a very good agreement with the theoretical calculations reported in the literature,³⁴ which predicted a semiconductor-to-metal transition above 20 GPa for bulk $\text{Mo}_{0.5}\text{W}_{0.5}\text{S}_2$. They are also well compatible with previous high-pressure measurements at room temperature on MoS_2 and WS_2 , which showed a metallic transition between 19 and 22 GPa for both samples.^{27,28} Interestingly, in the $\text{Mo}_{0.5}\text{W}_{0.5}\text{S}_2$ alloy the substitutional disorder of the crystal lattice, attested by the presence of the disorder-activated phonon peaks, does not strongly affect the electronic properties of the sample.

CONCLUSION

Transmission measurements were performed on a $\text{Mo}_{0.5}\text{W}_{0.5}\text{S}_2$ single crystal in the far-infrared range. The spectrum collected at ambient conditions enabled the classification of the observed peaks in terms of the lattice vibrational modes in comparison with the spectra of the binary constituents MoS_2 and WS_2 . High-pressure measurements allowed us to study the evolution of the lattice dynamics and to estimate the trend of the free carrier density up to 31 GPa. The behavior of the phonon peaks under pressure, very compatible with the Raman measurements reported in the literature,³³ confirmed the absence of structural transitions in the considered pressure range, while the abrupt increase of the spectral weight above 18 GPa indicated an increase in the charge carrier density. These results suggested the occurrence of an isostructural transition from a semiconducting to a metallic state in $\text{Mo}_{0.5}\text{W}_{0.5}\text{S}_2$ never experimentally investigated before. These results suggest the occurrence of an isostructural transition from a semiconducting to a metallic state in bulk $\text{Mo}_{0.5}\text{W}_{0.5}\text{S}_2$, in very good agreement with the theoretical calculations reported in the

literature,³⁴ which predicted the onset of the metallization process above 20 GPa. The observed effect is also coherent with previous studies on the binary compounds that found out a metallization pressure of ~ 19 ²⁷ and ~ 22 GPa²⁸ for MoS_2 and WS_2 , respectively, without relevant changes in the lattice symmetries. The compatibility between the metallization pressures of $\text{Mo}_{0.5}\text{W}_{0.5}\text{S}_2$ and its constituents suggests that substitutional disorder does not play a key role in the evolution of the electronic properties of the alloy under pressure.

ASSOCIATED CONTENT

Supporting Information

The Supporting Information is available free of charge at <https://pubs.acs.org/doi/10.1021/acs.jpcc.1c02315>.

Raman measurements on $\text{Mo}_{0.5}\text{W}_{0.5}\text{S}_2$; photoluminescence measurements on MoS_2 and WS_2 (PDF)

AUTHOR INFORMATION

Corresponding Authors

Francesca Ripanti – Department of Physics, Sapienza University of Rome, 00185 Rome, Italy; orcid.org/0000-0002-9505-740X; Email: francesca.ripanti@uniroma1.it

Paolo Postorino – Department of Physics, Sapienza University of Rome, 00185 Rome, Italy; orcid.org/0000-0002-3809-0676; Email: paolo.postorino@roma1.infn.it

Authors

Elena Stellino – Department of Physics and Geology, University of Perugia, 06123 Perugia, Italy

Giacomo Nisini – Department of Physics, Sapienza University of Rome, 00185 Rome, Italy

Francesco Capitani – Synchrotron SOLEIL, 91192 Gif-sur-Yvette, France; orcid.org/0000-0003-1161-7455

Caterina Petrillo – Department of Physics and Geology, University of Perugia, 06123 Perugia, Italy

Complete contact information is available at:

<https://pubs.acs.org/doi/10.1021/acs.jpcc.1c02315>

Notes

The authors declare no competing financial interest.

ACKNOWLEDGMENTS

We acknowledge SOLEIL for provision of synchrotron radiation facilities, and we would like to thank Dr. Anna Celeste and Dr. Bordondis Ferenc for assistance in using beamline SMIS.

REFERENCES

- (1) Yuan, L.; Ge, J.; Peng, X.; Zhang, Q.; Wu, Z.; Jian, Y.; Xiong, X.; Yin, H.; Han, J. A reliable way of mechanical exfoliation of large scale two dimensional materials with high quality. *AIP Adv.* **2016**, *6*, 125201.
- (2) Manzeli, S.; Ovchinnikov, D.; Pasquier, D.; Yazyev, O. V.; Kis, A. 2D transition metal dichalcogenides. *Nature Reviews Materials* **2017**, *2*, 17033.
- (3) Peng, J.; Wu, J.; Li, X.; Zhou, Y.; Yu, Z.; Guo, Y.; Wu, J.; Lin, Y.; Li, Z.; Wu, X.; Wu, C.; Xie, Y. Very Large-Sized Transition Metal Dichalcogenides Monolayers from Fast Exfoliation by Manual Shaking. *J. Am. Chem. Soc.* **2017**, *139*, 9019–9025.
- (4) Li, X.; Tao, L.; Chen, Z.; Fang, H.; Li, X.; Wang, X.; Xu, J. B.; Zhu, H. Graphene and related two-dimensional materials: Structure-property relationships for electronics and optoelectronics. *Appl. Phys. Rev.* **2017**, *4*, 021306.

- (5) Wang, Q. H.; Kalantar-Zadeh, K.; Kis, A.; Coleman, J. N.; Strano, M. S. Electronics and optoelectronics of two-dimensional transition metal dichalcogenides. *Nat. Nanotechnol.* **2012**, *7*, 699–712.
- (6) Jariwala, D.; Sangwan, V. K.; Lauhon, L. J.; Marks, T. J.; Hersam, M. C. Emerging Device Applications for Semiconducting Two-Dimensional Transition Metal Dichalcogenides. *ACS Nano* **2014**, *8*, 1102–1120.
- (7) Lu, C.; Chen, C. Structure-strength relations of distinct MoN phases from first-principles calculations. *Phys. Rev. Materials* **2020**, *4*, 044002.
- (8) Lu, C.; Chen, C. Indentation-strain stiffening in tungsten nitrides: Mechanisms and implications. *Phys. Rev. Materials* **2020**, *4*, 043402.
- (9) Heiße, F.; Kohler-Langes, F.; Rau, S.; Hou, J.; Junck, S.; Kracke, A.; Mooser, A.; Quint, W.; Ulmer, S.; Werth, G.; Blaum, K.; Sturm, S. High-Precision Measurement of the Proton's Atomic Mass. *Phys. Rev. Lett.* **2017**, *119*, 033001.
- (10) Yun, W. S.; Han, S. W.; Hong, S. C.; Kim, I. G.; Lee, J. D. Thickness and strain effects on electronic structures of transition metal dichalcogenides: 2H-MX₂ semiconductors (M = Mo, W; X = S, Se, Te). *Phys. Rev. B: Condens. Matter Mater. Phys.* **2012**, *85*, 033305.
- (11) Mak, K. F.; Lee, C.; Hone, J.; Shan, J.; Heinz, T. F. Atomically Thin MoS₂: A New Direct-Gap Semiconductor. *Phys. Rev. Lett.* **2010**, *105*, 136805.
- (12) Zhang, Y.; et al. Direct observation of the transition from indirect to direct bandgap in atomically thin epitaxial MoSe₂. *Nat. Nanotechnol.* **2014**, *9*, 111–115.
- (13) Xie, L. M. Two-dimensional transition metal dichalcogenide alloys: preparation, characterization and applications. *Nanoscale* **2015**, *7*, 18392–18401.
- (14) Zhao, Y.; Zhang, Z.; Ouyang, G. Band shift of 2D transition-metal dichalcogenide alloys: size and composition effects. *Appl. Phys. A: Mater. Sci. Process.* **2018**, *124*, 292.
- (15) Sahoo, S.; Gaur, A. P. S.; Ahmadi, M.; Guinel, M. J.-F.; Katiyar, R. S. Temperature-Dependent Raman Studies and Thermal Conductivity of Few-Layer MoS₂. *J. Phys. Chem. C* **2013**, *117*, 9042–9047.
- (16) Chakraborty, B.; Matte, H. S. S. R.; Sood, A. K.; Rao, C. N. R. Layer-dependent resonant Raman scattering of a few layer MoS₂. *J. Raman Spectrosc.* **2013**, *44*, 92–96.
- (17) Mahatha, S. K.; Patel, K. D.; Menon, K. S. R. Electronic structure investigation of MoS₂ and MoSe₂ using angle-resolved photoemission spectroscopy and ab initio band structure studies. *J. Phys.: Condens. Matter* **2012**, *24*, 475504.
- (18) Ulstrup, S.; Cabo, A. G.; Biswas, D.; Riley, J. M.; Dendzik, M.; Sanders, C. E.; Bianchi, M.; Cacho, C.; Matselyukh, D.; Chapman, R. T.; Springate, E.; King, P. D. C.; Miwa, J. A.; Hofmann, P. Spin and valley control of free carriers in single-layer WS₂. *Phys. Rev. B: Condens. Matter Mater. Phys.* **2017**, *95*, 041405.
- (19) Sekine, T.; Nakashizu, T.; Toyoda, K.; Uchinokura, K.; Matsuura, E. Raman scattering in layered compound 2H-WS₂. *Solid State Commun.* **1980**, *35*, 371–373.
- (20) Carvalho, B. R.; Malard, L. M.; Alves, J. M.; Fantini, C.; Pimenta, M. A. Erratum: Symmetry-Dependent Exciton-Phonon Coupling in 2D and Bulk MoS₂ Observed by Resonance Raman Scattering [Phys. Rev. Lett. **114**, 136403 (2015)]. *Phys. Rev. Lett.* **2016**, *116*, 089904.
- (21) Wang, Z.; Liu, P.; Ito, Y.; Ning, S.; Tan, Y.; Fujita, T.; Hirata, A.; Chen, M. Chemical Vapor Deposition of Monolayer Mo_{1-x}W_xS₂ Crystals with Tunable Band Gaps. *Sci. Rep.* **2016**, *6*, 21536.
- (22) Kim, J.-S.; Ahmad, R.; Pandey, T.; Rai, A.; Feng, S.; Yang, J.; Lin, Z.; Terrones, M.; Banerjee, S. K.; Singh, A. K.; Akinwande, D.; Lin, J.-F. Towards band structure and band offset engineering of monolayer Mo_xW_{1-x}S₂ via Strain. *2D Mater.* **2018**, *5*, 015008.
- (23) Qiao, X.-F.; Li, X.-L.; Zhang, X.; Shi, W.; Wu, J.-B.; Chen, T.; Tan, P.-H. Substrate-free layer-number identification of two-dimensional materials: A case of Mo_{0.5}W_{0.5}S₂ alloy. *Appl. Phys. Lett.* **2015**, *106*, 223102.
- (24) Zhang, X.; Qiao, X.-F.; Shi, W.; Wu, J.-B.; Jiang, D.-S.; Tan, P.-H. Phonon and Raman scattering of two-dimensional transition metal dichalcogenides from monolayer, multilayer to bulk material. *Chem. Soc. Rev.* **2015**, *44*, 2757–2785.
- (25) Stellino, E. Pressure evolution of the optical phonons of MoTe₂. *Il Nuovo Cimento C* **2020**, *43*, 1–8.
- (26) Yang, L.; Dai, L.; Li, H.; Hu, H.; Liu, K.; Pu, C.; Hong, M.; Liu, P. Pressure-induced metallization in MoSe₂ under different pressure conditions. *RSC Adv.* **2019**, *9*, 5794–5803.
- (27) Nayak, A. P.; Bhattacharyya, S.; Zhu, J.; Liu, J.; Wu, X.; Pandey, T.; Jin, C.; Singh, A. K.; Akinwande, D.; Lin, J.-F. Pressure-induced semiconducting to metallic transition in multilayered molybdenum disulfide. *Nat. Commun.* **2014**, *5*, 3731.
- (28) Nayak, A. P.; Yuan, Z.; Cao, B.; Liu, J.; Wu, J.; Moran, S. T.; Li, T.; Akinwande, D.; Jin, C.; Lin, J.-F. Pressure-Modulated Conductivity, Carrier Density, and Mobility of Multilayered Tungsten Disulfide. *ACS Nano* **2015**, *9*, 9117–9123.
- (29) Livneh, T.; Sterer, E. Resonant Raman scattering at exciton states tuned by pressure and temperature in 2H-MoS₂. *Phys. Rev. B* **2010**, *81*, 195209.
- (30) Livneh, T.; Reparaz, J. S.; Goñi, A. R. Low-temperature resonant Raman asymmetry in 2H-MoS₂ under high pressure. *J. Phys.: Condens. Matter* **2017**, *29*, 435702.
- (31) Brotons-Gisbert, M.; Segura, A.; Robles, R.; Canadell, E.; Ordejón, P.; Sánchez-Royo, J. F. Optical and electronic properties of 2H-MoS₂ under pressure: Revealing the spin-polarized nature of bulk electronic bands. *Phys. Rev. Materials* **2018**, *2*, 054602.
- (32) Zhuang, Y.; Dai, L.; Wu, L.; Li, H.; Hu, H.; Liu, K.; Yang, L.; Pu, C. Pressure-induced permanent metallization with reversible structural transition in molybdenum disulfide. *Appl. Phys. Lett.* **2017**, *110*, 122103.
- (33) Kim, J.-S.; Moran, S. T.; Nayak, A. P.; Pedazur, S.; Ruiz, I.; Ponce, G.; Rodriguez, D.; Henny, J.; Liu, J.; Lin, J.-F.; Akinwande, D. High pressure Raman study of layered Mo_{0.5}W_{0.5}S₂ ternary compound. *2D Mater.* **2016**, *3*, 025003.
- (34) Dong, J.; Ouyang, G. Thickness-Dependent Semiconductor-to-Metal Transition in Molybdenum Tungsten Disulfide Alloy under Hydrostatic Pressure. *ACS Omega* **2019**, *4*, 8641–8649.
- (35) Celeste, A.; Borondics, F.; Capitani, F. Hydrostaticity of pressure-transmitting media for high pressure infrared spectroscopy. *High Pressure Res.* **2019**, *39*, 608–618.
- (36) Chijioke, A. D.; Nellis, W. J.; Soldatov, A.; Silvera, I. F. The ruby pressure standard to 150 GPa. *J. Appl. Phys.* **2005**, *98*, 114905.
- (37) Caramazza, S.; Collina, A.; Stellino, E.; Ripanti, F.; Dore, P.; Postorino, P. First- and second-order Raman scattering from MoTe₂ single crystal. *Eur. Phys. J. B* **2018**, *91*, 1–7.
- (38) O'Neal, K. R.; Cherian, J. G.; Zak, A.; Tenne, R.; Liu, Z.; Musfeldt, J. L. High Pressure Vibrational Properties of WS₂ Nanotubes. *Nano Lett.* **2016**, *16*, 993–999.
- (39) Guo, X.; Chen, H.; Wen, X.; Zheng, J. Electron-phonon interactions in MoS₂ probed with ultrafast two-dimensional visible/far-infrared spectroscopy. *J. Chem. Phys.* **2015**, *142*, 212447.
- (40) Pike, N. A.; Van Troeye, B.; Dewandre, A.; Petretto, G.; Gonze, X.; Rignanese, G.-M.; Verstraete, M. J. Origin of the counterintuitive dynamic charge in the transition metal dichalcogenides. *Phys. Rev. B: Condens. Matter Mater. Phys.* **2017**, *95*, 201106.
- (41) Chen, Y.; Xi, J.; Dumcenco, D. O.; Liu, Z.; Suenaga, K.; Wang, D.; Shuai, Z.; Huang, Y.-S.; Xie, L. Tunable Band Gap Photoluminescence from Atomically Thin Transition-Metal Dichalcogenide Alloys. *ACS Nano* **2013**, *7*, 4610–4616.
- (42) Arcangeletti, E.; Baldassarre, L.; Di Castro, D.; Lupi, S.; Malavasi, L.; Marini, C.; Perucchi, A.; Postorino, P. Evidence of a Pressure-Induced Metallization Process in Monoclinic VO₂. *Phys. Rev. Lett.* **2007**, *98*, 196406.
- (43) Dore, P.; Sacchetti, A.; Postorino, P.; Congeduti, A.; Gorelli, F. A.; Ulivi, L. Evidence of Phase Separation in the P-T Phase Diagram of the La_{0.75}Ca_{0.25}MnO₃ Manganite by Infrared Measurements. *J. Supercond.* **2005**, *18*, 659–662.

(44) Postorino, P.; Congeduti, A.; Dore, P.; Sacchetti, A.; Gorelli, F.; Ulivi, L.; Kumar, A.; Sarma, D. D. Pressure Tuning of Electron-Phonon Coupling: The Insulator to Metal Transition in Manganites. *Phys. Rev. Lett.* **2003**, *91*, 175501.

(45) Calvani, P.; De Marzi, G.; Dore, P.; Lupi, S.; Maselli, P.; D'Amore, F.; Gagliardi, S.; Cheong, S-W. Infrared Absorption from Charge Density Waves in Magnetic Manganites. *Phys. Rev. Lett.* **1998**, *81*, 4504–4507.

(46) Liang, Y.; Huang, X.; Huang, Y.; Wang, X.; Li, F.; Wang, Y.; Tian, F.; Liu, B.; Shen, Z. X.; Cui, T. New Metallic Ordered Phase of Perovskite CsPbI₃ under Pressure. *Advanced Science* **2019**, *6*, 1900399.